JGR Solid Earth

RESEARCH ARTICLE
10.1029/2025JB031255

Mantle Flow and Crustal Deformation Revealed by Seismic Anisotropy in the Subduction Zone Beneath Myanmar

Enbo Fan[1,2], Mingming Jiang[1,3], Yinshuang Ai[1,3], Stephen S. Gao[2], Kelly H. Liu[2], Yumei He[1], Yiming Bai[4], Guangbing Hou[1], Yuan Ling[1], Chit Thet Mon[1], Myo Thant[5], and Kyaing Sein[6]

[1]Key Laboratory of Earth and Planetary Physics, Institute of Geology and Geophysics, Chinese Academy of Sciences, Beijing, China, [2]Department of Earth Sciences and Engineering, Missouri University of Science and Technology, Rolla, MO, USA, [3]College of Earth and Planetary Sciences, University of Chinese Academy of Sciences, Beijing, China, [4]Division of Mathematical Sciences, School of Physical and Mathematical Sciences, Nanyang Technological University, Singapore, Singapore, [5]Department of Geology, University of Yangon, Yangon, Myanmar, [6]Myanmar Geosciences Society, Yangon, Myanmar

Abstract The oblique convergence of the Indian and Eurasian plates drives significant deformation in the crust and mantle beneath Myanmar. However, the crustal deformation in the Indo-Burman Ranges (IBR) and mantle flow beneath Myanmar and adjacent areas remain unclear due to limited studies. We utilized data from the newly deployed second phase of the China-Myanmar Geophysical Survey of the Myanmar Orogen array to perform shear wave splitting analysis of PKS, SKKS, and SKS (XKS) phases. Our results, together with previous findings, provide new insights into mantle flow and crustal deformation across central Myanmar. In the IBR, we observed a transition from N-S oriented, structure-induced crustal anisotropy north of 21°N to trench-perpendicular, stress-induced crustal anisotropy in the south. Such a transition contributes to a significant southward decrease in XKS splitting times in the IBR, where the XKS fast orientations predominantly align in a trench-parallel direction. In the West Burma Terrane, the trench-parallel fast orientations gradually transition to nearly trench-perpendicular toward the Sibumasu Terrane (ST), along with the estimated depths of anisotropy, reflecting a change in the primary source of anisotropy from trench-parallel sub-slab flow to mantle wedge flow. The transitional fast orientations in the ST are influenced by three factors: corner flow induced by active subduction, absolute plate motion-driven flow, and the remnant Neo-Tethyan slab, which remains permeable to mantle flow at depths of 50–125 km. Our research advances the understanding of crust-mantle deformation in the subduction zone beneath Myanmar and provides valuable constraints for subduction dynamics studies in the region.

Plain Language Summary Myanmar lies at the boundary where the Indian and Eurasian plates converge at an angle, with the subduction of the Indian plate causing significant deformation in the Earth's crust and mantle. This deformation affects how seismic waves travel, causing shear waves to split into fast and slow waves. However, limited studies have left crustal deformation in the Indo-Burman Ranges (IBR) and mantle flow beneath Myanmar and nearby areas poorly understood. To address this, we analyzed data from a newly deployed seismic network in central Myanmar. By studying how shear waves split and combining our findings with previous research, we provided new insights into mantle flow and crustal deformation in the region. In the IBR, crustal deformation is attributable to geological structures in the north and stress in the south. The primary mantle flow transitions from beneath the subducting Indian slab in the West Burma Terrane to the mantle wedge above the slab in the Sibumasu Terrane (ST). Beneath the ST, mantle flow is influenced by three factors: Eurasian plate motion, Indian plate subduction, and a remnant slab that allows mantle material to pass through. Our findings improve understanding of crust-mantle interactions and subduction-driven deformation in Myanmar.

Key Points:

- Southward-decreasing splitting times in the Indo-Burman Ranges reflect a shift from structure- to stress-induced crustal anisotropy
- The primary source of anisotropy shifts from the sub-slab mantle in the West Burma Terrane to the mantle wedge in the Sibumasu Terrane
- Transitional fast orientations in Sibumasu result from absolute plate motion, subduction, and a remnant slab permeable to mantle flow

Supporting Information:

Supporting Information may be found in the online version of this article.

Correspondence to:

Y. Ai and S. S. Gao,
ysai@mail.iggcas.ac.cn;
sgao@mst.edu

Citation:

Fan, E., Jiang, M., Ai, Y., Gao, S. S., Liu, K. H., He, Y., et al. (2025). Mantle flow and crustal deformation revealed by seismic anisotropy in the subduction zone beneath Myanmar. *Journal of Geophysical Research: Solid Earth*, *130*, e2025JB031255. https://doi.org/10.1029/2025JB031255

Received 24 JAN 2025
Accepted 15 AUG 2025

Author Contributions:

Conceptualization: Enbo Fan, Mingming Jiang, Yinshuang Ai, Stephen S. Gao
Data curation: Enbo Fan, Mingming Jiang, Yumei He, Guangbing Hou, Yuan Ling, Chit Thet Mon, Myo Thant, Kyaing Sein
Formal analysis: Enbo Fan
Funding acquisition: Enbo Fan, Mingming Jiang, Yinshuang Ai, Stephen S. Gao, Kelly H. Liu, Yumei He
Investigation: Enbo Fan, Mingming Jiang, Yinshuang Ai, Yumei He, Yiming Bai, Guangbing Hou, Yuan Ling, Chit Thet Mon, Myo Thant, Kyaing Sein
Methodology: Stephen S. Gao, Kelly H. Liu
Project administration: Mingming Jiang, Yinshuang Ai

1. Introduction

Subduction of the lithosphere into the mantle leads to severe deformation of both the subducting lithosphere and the surrounding crust and mantle. Understanding these deformation patterns is essential for comprehending the subduction dynamics and tectonic evolution of subduction zones. Myanmar is located on the eastern side of the India-Eurasia convergent boundary, beneath which the eastward-dipping subducting Indian slab is clearly

Resources: Yinshuang Ai, Stephen S. Gao
Software: Stephen S. Gao, Kelly H. Liu
Supervision: Yinshuang Ai
Validation: Yinshuang Ai, Stephen S. Gao, Kelly H. Liu
Visualization: Enbo Fan
Writing – original draft: Enbo Fan
Writing – review & editing: Enbo Fan, Mingming Jiang, Yinshuang Ai, Stephen S. Gao, Kelly H. Liu, Yumei He, Yiming Bai

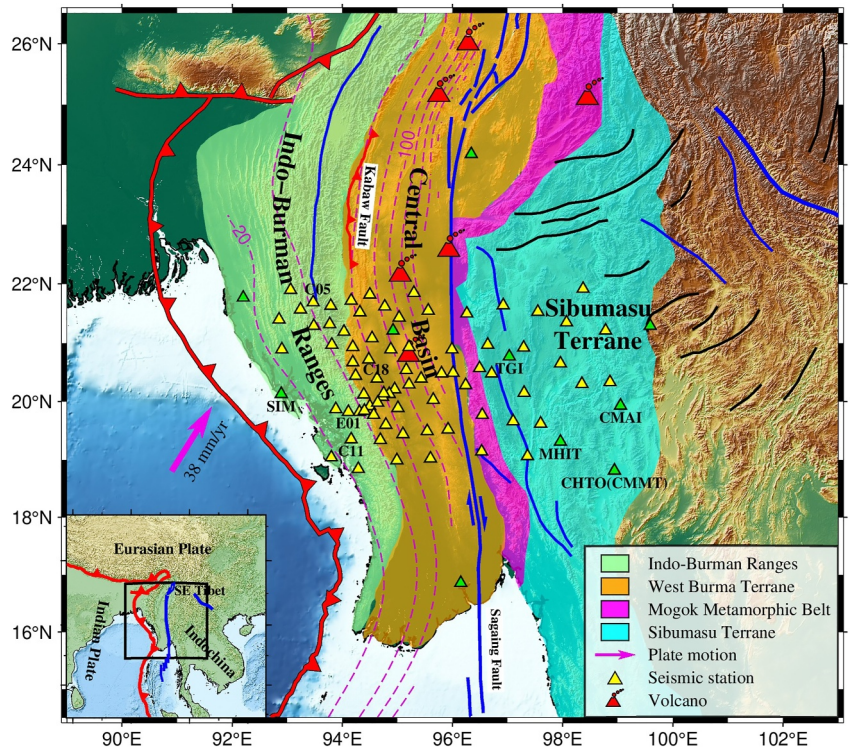

Figure 1. Topographic map of Myanmar and adjacent regions showing tectonic divisions and distribution of seismic stations. Yellow triangles represent the locations of seismic stations from the second phase of the China-Myanmar Geophysical Survey of the Myanmar Orogen, while green triangles indicate stations from the Seismological Facility for the Advancement of Geoscience (SAGE). Dashed purple lines represent slab contours based on the Slab2 model (Hayes et al., 2018). The purple arrow indicates the motion of the Indian plate relative to eastern Myanmar (Mallick et al., 2019). Major faults are shown, with thrust faults in red, dextral strike-slip faults in blue, and sinistral strike-slip faults in black. The inset map shows the location of the study area in a broader context.

revealed by earthquake locations and seismic tomography (e.g., Hurukawa et al., 2012; Li et al., 2008; Mon et al., 2023; Yao et al., 2021). Therefore, it is an ideal region for studying crustal and mantle deformation and subduction dynamics.

From west to east, Myanmar is composed of four tectonic units (Figure 1), the Indo-Burman Ranges (IBR), an accretionary wedge formed by the subduction of the Indian plate (e.g., Garzanti et al., 2013; Morley et al., 2020); the West Burma Terrane (WBT), comprising primarily a Paleogene-Recent sedimentary basin and containing a series of Miocene-Quaternary volcanoes (Lee et al., 2016; Morley et al., 2021); the Mogok Metamorphic Belt, mainly composed of high-grade metamorphic rocks and granites (e.g., Searle et al., 2017); and the Sibumasu Terrane (ST), a ribbon continent composed of Precambrian to Late Mesozoic strata (Cai et al., 2017; Morley, 2018). GPS studies indicate that the Indian plate is currently obliquely converging with the Eurasian plate along the megathrust fault on the western side of Myanmar at a rate of approximately 38 mm/year toward the NNE direction (Mallick et al., 2019). This convergence process dominates the present-day tectonic activity and deformation in Myanmar.

The IBR features numerous folds and faults aligned with the trend of the mountain range (e.g., Morley et al., 2020; Wang et al., 2014). The maximum principal stress direction in the crust is oriented perpendicular to this trend (Lindsey et al., 2023; Mon et al., 2020), while crustal fast orientations are parallel to it (Fan et al., 2021), indicating that the crustal anisotropy is predominantly controlled by geological structures. However, topographic data show that from 21°N southward, the elevation of the IBR decreases (Morley et al., 2020) and its width narrows significantly (Figure 1), raising questions about whether the structure-induced anisotropy persists further south. Additionally, mantle transition zone studies suggest that the subducted Indian plate beneath Myanmar at 21°N has torn (Bai et al., 2020), potentially altering mantle flow in the surrounding region (e.g., Guillaume et al., 2010; Liu & Pysklywec, 2023; Lynner et al., 2017; Paul et al., 2014). However, due to the lack of seismic anisotropy studies

in this region, the impact of slab tearing on material transport and mantle flow remains unclear. Furthermore, multiple competing theories regarding the mechanisms driving mantle flow beneath the ST and adjacent regions, including E-W mantle flow induced by slab rollback, mantle flow driven by absolute plate motion (APM), and corner flow due to Indian plate subduction (e.g., Fan et al., 2021; Z. Huang et al., 2015; Islam et al., 2024; Kong et al., 2018; Yu et al., 2018), complicate the understanding of mantle dynamics in this region. Recent teleseismic tomography has revealed a remnant eastward-dipping Neo-Tethyan oceanic lithosphere beneath the ST (Yang et al., 2022). This remnant slab could represent a new driving mechanism for mantle flow in this region. Determining which mechanism is dominant, or if they act in combination, requires further studies on seismic anisotropy in the region.

Deformation in the crust and upper mantle can produce seismic anisotropy, whereby seismic wave velocities vary with propagation direction or polarization orientation. In the upper crust, seismic anisotropy is commonly attributed to shape preferred orientation, which arises from the alignment of fluid-saturated microcracks under the influence of stress or structural controls (e.g., Crampin & Peacock, 2008; Leary et al., 1990). In contrast, seismic anisotropy in the lower crust and upper mantle is primarily attributed to lattice preferred orientation, resulting from the strain-induced alignment of anisotropic minerals such as mica, amphibole, and olivine (e.g., Almqvist & Mainprice, 2017; Karato et al., 2008; Savage, 1999). Measuring the splitting parameters of PKS, SKKS, and SKS phases (collectively referred to as XKS) is an effective method for acquiring seismic anisotropy of subsurface media. When an S-wave propagates through an anisotropic medium, it splits into two quasi-S waves with orthogonal polarizations and different velocities. The delay time between the fast and slow S-waves (splitting time δt) reflects the strength of anisotropy, while the polarization direction of the fast S-wave (fast orientation φ) reveals the orientation of aligned fluid-saturated microcracks or the fast axis of anisotropic minerals. These measurements are essential for understanding crustal anisotropy mechanisms and determining mantle flow directions.

After completing the first phase of the China-Myanmar Geophysical Survey of the Myanmar Orogen (CMGSMO) temporary seismic array observation in February 2018 (e.g., Mon et al., 2020), we conducted the nearly two-year second phase of the CMGSMO temporary seismic array observation. Seismic stations were deployed south of the first phase array and commenced data recording in January 2019 (station locations shown in Figure 1, station names in Figure S1 in Supporting Information S1), resulting in the acquisition of a large amount of valuable seismic data. Utilizing data from the second phase of the CMGSMO temporary seismic array and nearby publicly accessible stations, we conducted shear wave splitting (SWS) analysis of XKS phases, analyzed crustal anisotropy specifically for stations in the IBR, and estimated anisotropy depth across the study area. These analyses revealed the spatial pattern of seismic anisotropy, providing effective constraints on crustal and mantle deformation mechanisms, as well as subduction dynamics within the complex double-subduction and slab-tear structures of the subduction zone beneath Myanmar. More broadly, the new seismic anisotropy results, combined with previous findings from SE Tibet and the Indochina Peninsula, offer significant insights into mantle flow and geodynamic processes in and around Myanmar.

2. Data and Method

2.1. Station Distribution

The seismic data used in this study were primarily collected from the newly deployed second phase of the CMGSMO temporary seismic array, which operated in central Myanmar from January 2019 to October 2020. This array comprises 75 broadband seismic stations distributed across major tectonic units, including the IBR, the WBT, the Mogok Metamorphic Belt, and the ST, within the latitude range of 18.5°–22°N, forming a two-dimensional network (Figure 1). Each station was equipped with a Trillium 120 PA seismometer and a Taurus digitizer, with station spacing ranging from 10 to 80 km. Additionally, we processed seismic data from 11 publicly accessible stations provided by the Seismological Facility for the Advancement of Geoscience (SAGE), located in the vicinity of the second phase of the CMGSMO array (Figure 1 and Figure S1 in Supporting Information S1). The SWS measurements at stations CHTO, CMAI, CMMT, MHIT, and SIM have been previously reported (Liu et al., 2019; Yu et al., 2018), and we have updated these measurements with data collected up to October 2022.

2.2. Shear Wave Splitting

We utilized the XKS phases to obtain the SWS parameters (splitting time and fast orientation). The advantages of these phases are that after the P-wave travels through the outer core and reaches the mantle, converting to an S-wave, its initial polarization direction is determined, and it retains only the anisotropic information beneath the receiver side. We selected earthquakes with epicentral distances between 84° and 180° and magnitudes greater than 5.6, except for those with focal depths exceeding 100 km, for which a minimum magnitude of 5.5 was required. For the selected earthquakes, we rotated the two horizontal components of the waveforms into radial and transverse components and applied a bandpass filter of 0.04–0.5 Hz. The waveform window for calculating the SWS parameters was chosen from 5 s before to 20 s after the theoretical phase arrival time, and waveforms with a signal-to-noise ratio lower than four on the radial component were discarded (Liu & Gao, 2013). We then applied the minimum energy method (Silver & Chan, 1991) to the remaining waveforms. This technique identifies the pair of splitting parameters that minimize the energy on the corrected transverse component, yielding the preliminary SWS measurements. To estimate uncertainties in these parameters, we followed the approach of Silver and Chan (1991), using the inverse F-test at the 95% confidence level.

To ensure the quality of the SWS results, we first automatically ranked the preliminary results (Liu et al., 2008) and then manually inspected each ranked result. By adjusting the waveform window and filter band, we mitigated the interference of noise on the XKS signal. The results were then classified into four categories: A, B, C, and N. Category A represents excellent SWS results, characterized by the following criteria: (a) Distinct XKS signals on the original radial and transverse components; (b) Nearly complete elimination of energy on the corrected transverse component; (c) An elliptical particle motion pattern initially, transitioning to a linear or nearly linear pattern after correction; and (d) Small standard deviations for both fast orientation and splitting time (Figure S2 in Supporting Information S1). Category B represents good SWS results that are slightly inferior to Category A. Category C represents poor-quality results that were discarded because they did not meet all four criteria simultaneously. Category N represents null measurements, where the XKS signal was distinct on the original radial component but exhibited little to no energy on the transverse component (Figure S3 in Supporting Information S1).

3. Results

We obtained a total of 731 well-defined (Category A or B) SWS measurements from 80 out of 86 stations, including 32 PKS, 206 SKKS, and 493 SKS splitting measurements. All splitting measurements exhibit standard deviations of ≤16° in fast orientation and ≤0.5 s in splitting time. Over 80% of the measurements have standard deviations of ≤10° in fast orientation and ≤0.3 s in splitting time. Note that the standard deviation estimates of Silver and Chan (1991) may be underestimated, as noted by Walsh et al. (2013).

These measurements were derived from 143 earthquake events, each contributing at least one splitting measurement. The SKS splitting measurements are primarily from earthquake events with back-azimuths between 100° and 130°, and the SKKS measurements primarily come from events with back-azimuths in the ranges of 200°–220°, 240°–260°, and 280°–300°. The fewer PKS splitting measurements mainly originate from earthquake events with back-azimuths around 20° and 345°. Overall, the back-azimuthal coverage of the earthquake events is robust (Figure 2).

The average splitting time and fast orientation for the study region are 1.24 ± 0.43 s and −16.6 ± 20.4°, respectively. The average splitting times for the study region and for each of the stations (Table S1) were calculated as the arithmetic mean of all measured values, whereas the average fast orientations for the study region and the individual stations (Table S1) were computed using circular (von Mises) statistics (Gerst, 2003). The station-averaged splitting times at most stations are comparable to the regional average. However, Station C05, located in the northern IBR, exhibits a significantly larger station-averaged splitting time of 2.3 ± 0.5 s (red star in Figure 3), more than one second higher than the regional average. This large splitting time is consistent with the XKS splitting measurements reported by Fan et al. (2021) in the IBR. The fast orientations observed at stations in the IBR, WBT, Mogok Metamorphic Belt, and western ST predominantly align with the strike of the subducting slab. Farther east, north of 19.5°N, the fast orientations exhibit a counterclockwise rotation with increasing distance eastward, gradually becoming perpendicular to the strike of the subducting slab. South of 19.5°N, the fast orientations undergo a significant, large-angle deflection (Figure 3).

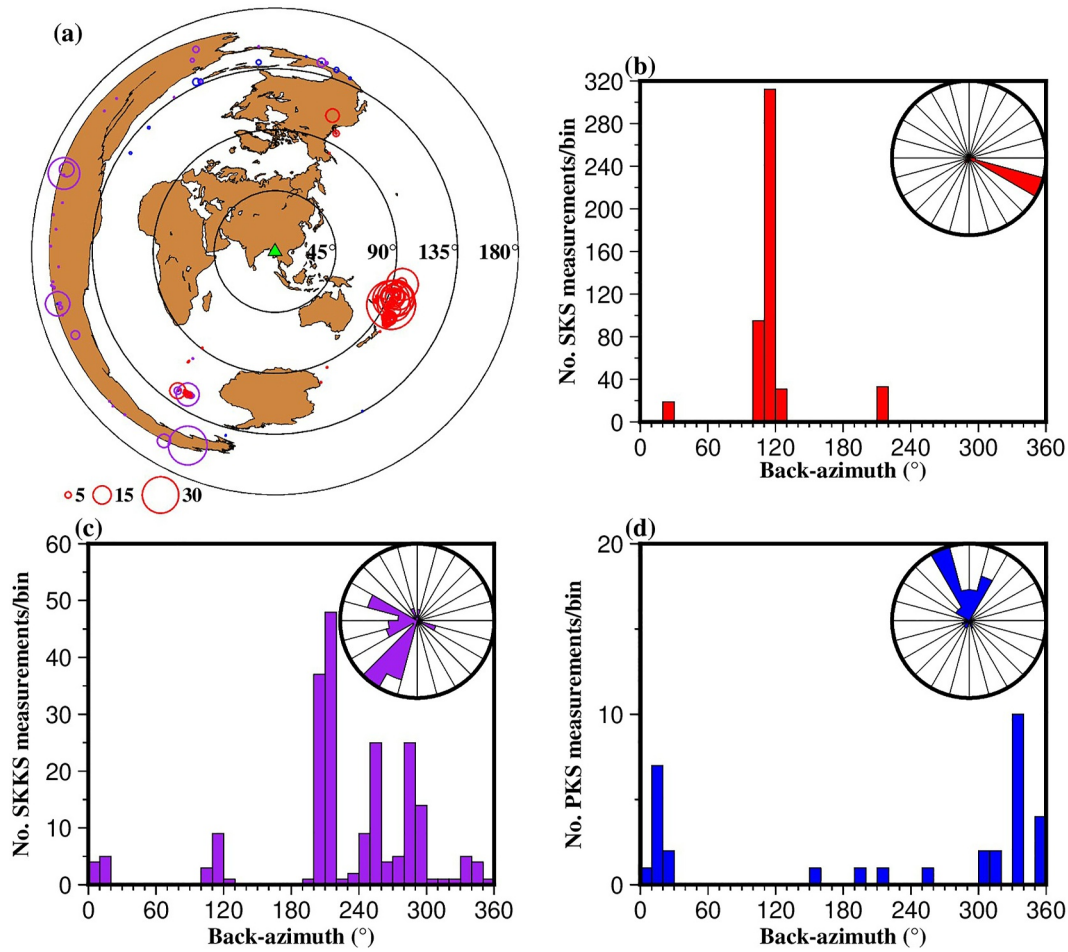

Figure 2. Teleseismic event distribution and back-azimuth coverage for shear wave splitting analysis. (a) Events used for SKS (red circles), SKKS (purple circles), and PKS (blue circles) splitting analysis. The size of each circle represents the number of splitting measurements obtained from the corresponding event. The green triangle denotes the study area. (b–d) Histograms and rose diagrams illustrating the back-azimuth distribution of events used in (b) SKS, (c) SKKS, and (d) PKS splitting analysis, respectively.

A negative correlation between splitting time and the dominant frequency of the corresponding phase has been reported in previous studies (e.g., Huang et al., 2011, 2017). To examine this relationship in our data set, we calculated the dominant frequency for each XKS phase and performed a linear regression analysis with the corresponding splitting times. The analysis yields a Pearson correlation coefficient of −0.17, indicating a very weak linear relationship (Figure S4 in Supporting Information S1). Although splitting times exceeding 2.5 s are exclusively found in the lower frequency range, small splitting times also occur within the same frequency band. Therefore, we conclude that the influence of signal frequency on the splitting times is minimal in our observations.

We obtained a total of 243 null measurements (Category N) at 59 stations. At most stations, the two directions of the null measurements (corresponding to the event back-azimuth and the direction perpendicular to the back-azimuth) are either parallel or perpendicular to the fast orientations (Figure S5a in Supporting Information S1). At stations C18 and TGI, the null measurements exhibit two dominant directions (Figure S5a in Supporting Information S1). However, when projecting the null measurements from these two stations to their corresponding 200 km depth ray-piercing points (Fan et al., 2021), the directions of the null measurements align parallel or perpendicular to the surrounding XKS fast orientations (Figure S5b in Supporting Information S1). Therefore, we assert that the null measurements in this study region result from event back-azimuths being nearly parallel or perpendicular to the fast orientation of the anisotropic medium, in which case the traversing shear waves do not

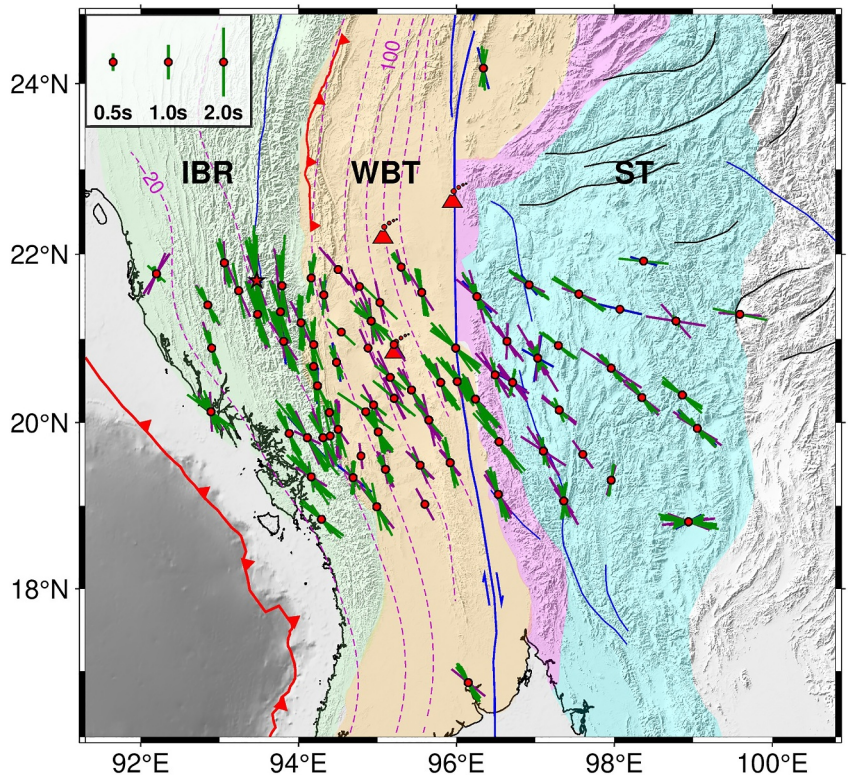

Figure 3. Map illustrating all SKS (green bars), SKKS (purple bars), and PKS (blue bars) splitting measurements, plotted at the station locations (red circles). The orientation of each bar represents the fast orientation, and its length corresponds to the splitting time, as indicated in the legend. Abbreviations: IBR: Indo-Burman Ranges, ST: Sibumasu Terrane, WBT: West Burma Terrane.

undergo splitting, leading to null measurements. Consequently, we did not observe any pure null measurements indicative of an isotropic medium in this study region.

At most stations, the splitting times and fast orientations of individual splitting measurements remain consistent within the uncertainties (examples from some stations are shown in Figures S6 and S7 in Supporting Information S1). However, at certain stations, we observe variations in splitting times and fast orientations with back-azimuth, though these variations do not exhibit the 90° periodicity that would be expected in a two-layer anisotropic model (Figures S8 and S9 in Supporting Information S1). Additionally, null measurements were recorded at some of these stations. In a two-layer anisotropic model, an S-wave with arbitrary polarization would always undergo splitting after passing through the two anisotropic layers, making it unlikely to observe null measurements. Therefore, the lack of 90° periodicity in the variations of splitting parameters with back-azimuth, combined with the presence of null measurements, suggests that a two-layer anisotropic model cannot explain the observed splitting parameters.

It is important to note that we cannot completely rule out the possibility of a two-layer anisotropic structure at all stations. Approximately 68% of the splitting measurements are derived from SKS phases, which predominantly arrive from back-azimuths between 100° and 130° (Figure 2). Consequently, some stations (e.g., C25 and C33 in Figures S6 and S7 in Supporting Information S1) have limited back-azimuthal coverage, which may reduce the ability to resolve complex anisotropic structures beneath them. Therefore, although a two-layer anisotropic model appears unlikely, its presence cannot be completely excluded. Fortunately, the addition of SKKS and PKS phases greatly improved the azimuthal coverage for most of the stations.

When projecting the splitting measurements from the stations exhibiting variations in splitting parameters with back-azimuth to their corresponding 200 km depth ray-piercing points (Fan et al., 2021), we find that the splitting measurements at nearby piercing point locations are consistent with each other (Figures S8 and S9 in Supporting Information S1). This indicates that the observed variations in splitting parameters are controlled by the ray-

piercing point locations. The splitting parameters systematically reveal lateral variations in anisotropy across the study region, and a single anisotropic layer with a horizontal symmetry axis can sufficiently explain the observed results.

4. Discussion

4.1. Estimating the Depth of Anisotropy

The SWS measurements reflect the integrated effect of anisotropic media along the ray path. Seismic tomographic studies reveal the presence of a subducting Indian slab beneath the study area (e.g., Yang et al., 2022; Yao et al., 2021; Zhang et al., 2021; Zheng et al., 2020). As a result, the converted S-waves of the XKS phases traverse the mantle beneath the subducting slab, the slab itself, the mantle wedge above the subducting slab, and the crust, all of which may contribute to the observed anisotropy. We combined the XKS splitting results from this study with those from adjacent regions (Fan et al., 2021; Liu et al., 2019; Yu et al., 2018) and employed the spatial coherence method (detailed in Supporting Information S1) to estimate the depths of anisotropy beneath the IBR, WBT, and the combined region of the Mogok Metamorphic Belt and ST (Figure 4).

Our analysis indicates that the depth of anisotropy in the IBR is 235 km (Figure 4b), considerably greater than the 20–60 km depths of the upper interface of the subducting slab in this region (Hayes et al., 2018), suggesting that sub-slab mantle is the primary source of anisotropy under the IBR. For the WBT, the optimal estimated depth of anisotropy is 190 km, with another possible depth of 320 km (Figure 4c), both of which are deeper than the 60–160 km depths of the upper interface of the subducting slab (Hayes et al., 2018). Moreover, the SWS measurements from local earthquakes in the WBT show an average splitting time of 0.35 ± 0.15 s, which has been attributed to mantle wedge anisotropy induced by corner flow (Fan et al., 2024). However, this value is less than 30% of the regional average XKS splitting time of 1.24 ± 0.43 s. Additionally, the XKS fast orientations in the WBT consistently align parallel to the trench, in contrast to the fast orientations from local earthquakes reported by Fan et al. (2024), which exhibit both trench-parallel and trench-perpendicular directions. These contrasting observations suggest that mantle wedge anisotropy is unlikely to be the primary source of anisotropy beneath the WBT. Another possible source of the observed XKS splitting is anisotropy in the subducted slab. Appini et al. (2025) demonstrated that a dipping slab with intrinsic anisotropy can account for the observed splitting parameters in the Ryukyu subduction zone. Such a structure, characterized by a tilted symmetry axis, can lead to a 180° periodic variation in XKS splitting parameters at a single station (e.g., Liu & Gao, 2013). However, our XKS observations do not convincingly display this periodic behavior (Figures S6–S9 in Supporting Information S1). Taken together, although both the mantle wedge and the slab may contribute to anisotropy, the anisotropy in the WBT primarily originates from the sub-slab mantle, consistent with Fan et al. (2021).

In the combined region of the Mogok Metamorphic Belt and ST, the estimated depth of anisotropy is 125 km (Figure 4d), exceeding the lithospheric thickness of ~50 km (Pasyanos et al., 2014) but shallower than the upper interface of the subducting Indian slab in this region (e.g., Yang et al., 2022; Yao et al., 2021). A 50-km-thick layer with 4% anisotropy would produce a splitting time of ~0.5 s (e.g., Gao et al., 2010; Silver, 1996), which does not fully account for the average XKS splitting time of 1.24 ± 0.43 s. Furthermore, the fast orientations near the faults do not correlate with the fault strike. Around 23°N, where the strike of the Mogok Metamorphic Belt changes significantly, the XKS fast orientations also fail to exhibit a consistent correlation with its structural trend (Figure 4a). Additionally, the splitting times at stations close to the faults do not exhibit a significant increase (Figures 3 and 4a). These findings suggest that the lithospheric contribution to the anisotropy is relatively minor. Based on these arguments, we propose that from the WBT to the Mogok Metamorphic Belt and ST, the dominant source of the anisotropy transitions from the mantle beneath the slab to the mantle wedge above the slab.

4.2. Spatial Variations in Seismic Anisotropy Beneath the IBR

By projecting the splitting measurements obtained at stations in different regions to their corresponding ray-piercing points at depths determined in Section 4.1, the spatial variations in splitting measurements become more evident. One of the most striking features is the anomalously large splitting times in the northern part of the IBR (Figure 5). Fan et al. (2021) reported XKS splitting times exceeding 2 s and the presence of N-S oriented crustal anisotropy in the IBR (Figure 5). They interpreted the anomalously large XKS splitting times as the combined effect of anisotropy generated by trench-parallel mantle flow beneath the subducting slab and lithospheric anisotropy aligned parallel to the structural orientation of the IBR. Interestingly, the anomalously large

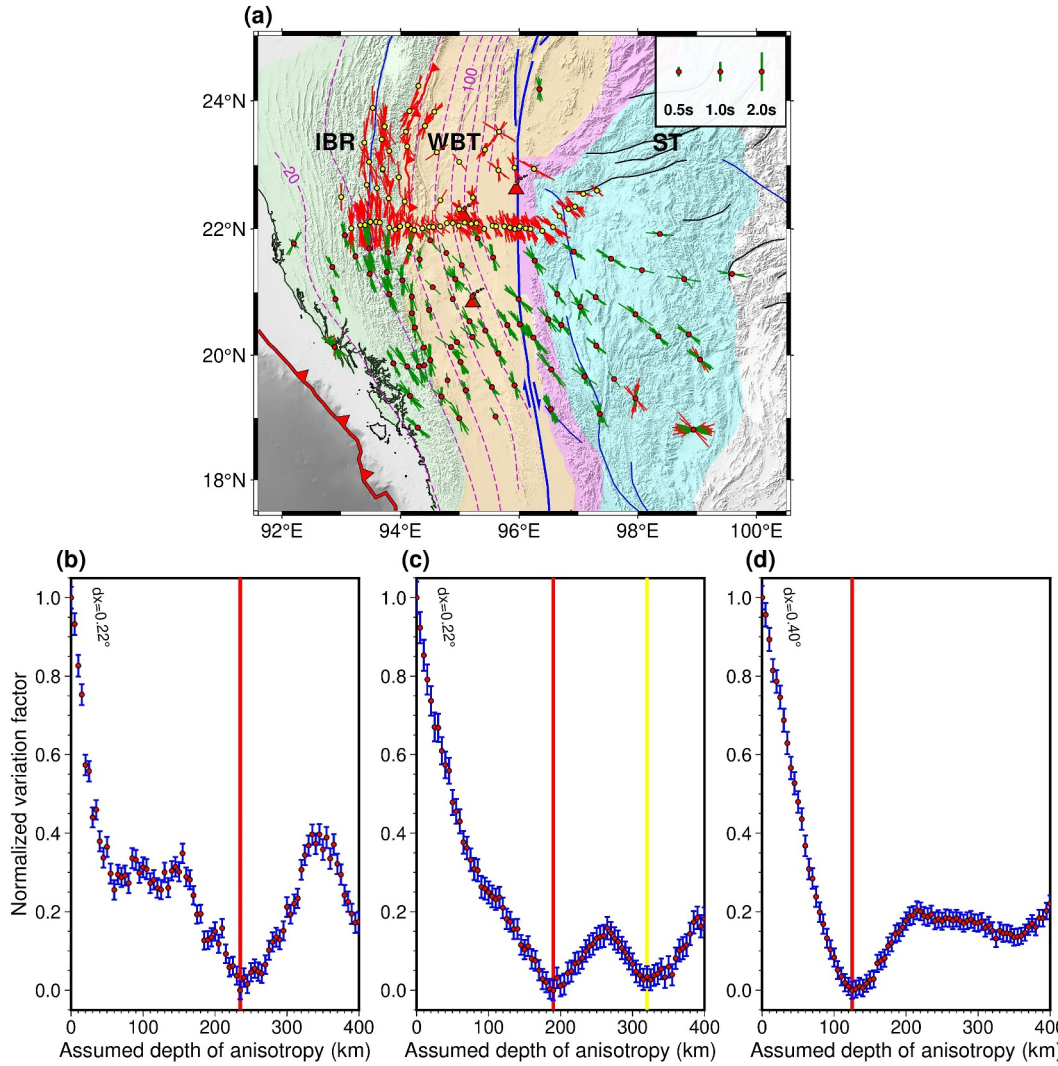

Figure 4. Estimated anisotropy depths from XKS splitting measurements. (a) Distribution of splitting measurements used to compute variation factors, plotted at the station locations. Green bars denote measurements from this study, while red bars represent measurements from previous studies (Fan et al., 2021; Liu et al., 2019; Yu et al., 2018). (b–d) Normalized variation factors computed using splitting measurements from stations in the (b) Indo-Burman Ranges (IBR; green region in panel a), (c) West Burma Terrane (WBT; yellow region in panel a), and (d) Mogok Metamorphic Belt (purple region in panel a) and Sibumasu Terrane (ST; blue region in panel a). The red lines indicate the estimated anisotropy depth corresponding to the minimum variation factor, while the yellow line in panel (c) represents an additional potential anisotropy depth corresponding to a local minimum in the variation factor. "dx" refers to the block size used for variation factor calculations.

splitting times do not extend to the southern part of the IBR, reflecting significant spatial variations in anisotropy beneath this region (Figure 5). P-wave receiver function and seismic velocity studies indicate a layered structure beneath the IBR, consisting of the Myanmar crust, the subducting Indian slab, and the sub-slab mantle from top to bottom (Bai et al., 2021; Zheng et al., 2020). We propose that the observed variations in anisotropy can be attributed to the influences of these distinct layers.

To investigate the crustal anisotropy in the IBR, we extracted radial P-wave receiver functions from seismic stations distributed across the region and analyzed the P-to-S converted phase (Pms) from the Moho discontinuity (see Supporting Information S1 for detailed methodology and data description). At stations C11, SIM_MM, and SIM_RM, which are situated in the southern IBR, where the XKS splitting times are smaller than in the northern part (Figure 5), the obtained delay times and fast orientations of the crust are (0.68 s, 66.8°), (0.36 s, 59.4°), and (0.28 s, 52.7°), respectively (Figures S10–S12 in Supporting Information S1). The crustal fast orientations at these

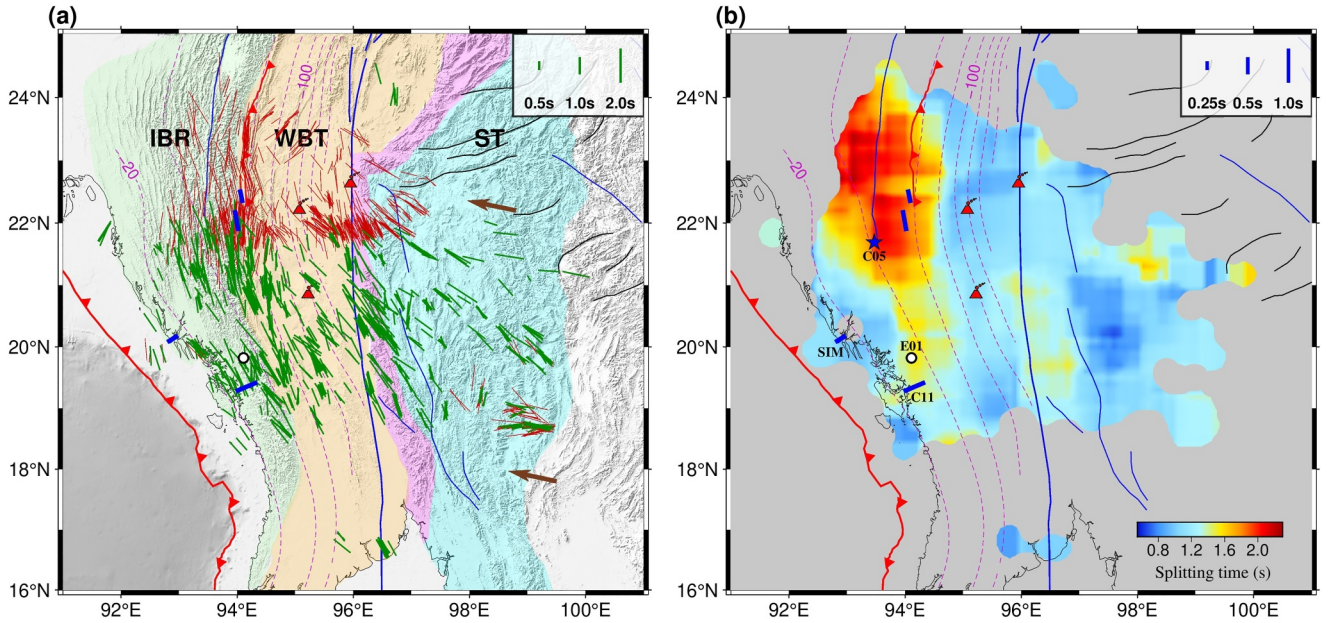

Figure 5. (a) XKS splitting measurements plotted at their corresponding ray-piercing points. The splitting measurements from stations in the Indo-Burman Ranges (IBR), the West Burma Terrane (WBT), and the combined region of the Mogok Metamorphic Belt and the Sibumasu Terrane (ST) are plotted at ray-piercing depths of 235 km, 190 km, and 125 km, respectively. These depths are derived by estimating anisotropy depths within different tectonic divisions, corresponding to the minimum values of the variation factors (see Figure 4). The brown arrows indicate the absolute plate motion of the Eurasian Plate at ~23 mm/yr in the hotspot reference frame (Gripp & Gordon, 2002). Blue bars represent crustal anisotropy results, with lengths corresponding to splitting times as indicated by the scale bar in panel (b). Red bars represent previous XKS splitting measurements (Fan et al., 2021; Liu et al., 2019; Yu et al., 2018), while green bars represent XKS splitting measurements from this study. (b) Spatially averaged XKS splitting times calculated based on measurements plotted at the ray-piercing points shown in panel (a). The blue star marks the location of Station C05. Two N-S oriented blue bars in the northern IBR and two trench-perpendicular blue bars in the southern IBR represent crustal anisotropy results from Fan et al. (2021) and this study, respectively. The white circle represents the crustal anisotropy result at Station E01, which indicates a nearly isotropic crust.

stations are nearly perpendicular to both the strike of the subducting slab and the XKS fast orientations (Figure 5). These observations suggest a two-layer anisotropic structure beneath the stations: the upper layer (crust) has a fast orientation perpendicular to the slab strike, while the lower layer has a fast orientation parallel to the slab strike with a larger splitting time. In the case of this special two-layer anisotropic structure, the splitting parameters do not exhibit the 90° periodic variation with back-azimuth that is characteristic of two-layer anisotropy. Instead, the observed splitting behavior resembles that of a single-layer anisotropy. The measured XKS fast orientation corresponds to the fast orientation of the lower layer medium (with a larger splitting time), and the splitting time is the absolute difference between the splitting times of the two layers (e.g., Liu & Gao, 2013; Silver & Savage, 1994). In contrast to the southern IBR, the crustal fast orientation is N-S in the northern IBR (Fan et al., 2021), which is consistent with the XKS fast orientations in this area (Figure 5). In the case of this two-layer structure, the XKS splitting time is equal to the sum of the splitting times of each layer along the ray path. The consistency between the crustal and XKS fast orientations in the northern IBR results in a significantly increased XKS splitting time compared to the area to the south, where the crustal fast orientations differ by nearly 90° from the XKS fast orientations.

At Station E01, the Pms arrival times on the radial P-wave receiver functions vary little with the back-azimuth, suggesting that the crust beneath this station is nearly isotropic (Figure 5 and Figure S13 in Supporting Information S1). Consequently, the XKS splitting measurements at E01 primarily reflect the anisotropy below the crust. The average XKS splitting time at E01 is 2.0 ± 0.5 s (Figure S9 in Supporting Information S1), which falls between the values at stations C11 (1.3 ± 0.4 s; Figure S8 in Supporting Information S1) and SIM (1.0 ± 0.3 s; Figure S7 in Supporting Information S1), both affected by crustal anisotropy with fast orientations perpendicular to the slab strike, and at Station C05 (2.3 ± 0.5 s; Figure S8 in Supporting Information S1) in the northern IBR, influenced by N-S oriented crustal anisotropy. This observation highlights the significant influence of crustal anisotropy variations in the IBR on the observed XKS splitting times. When the crustal fast orientations align with the surrounding XKS fast orientations, as at Station C05, the observed XKS splitting times increase (Figure 5). Conversely, when the crustal fast orientations are perpendicular to the surrounding XKS fast orientations, as at

stations C11 and SIM, the observed XKS splitting times decrease (Figure 5). Notably, the sum of the average XKS splitting time (1.3 s) and the crustal delay time (0.68 s) at C11 equals 1.98 s, which closely matches the average XKS splitting time at E01 (2.0 s), suggesting that the difference in the average XKS splitting times between C11 and E01 can be almost entirely attributed to the contrasting crustal anisotropy.

The N-S crustal fast orientations observed in the northern IBR by Fan et al. (2021) are parallel to the structural trend of the mountain range (Figure 5) and the strike of the faults (Gahalaut et al., 2013; Wang et al., 2014) while being perpendicular to the direction of compressive strain (Lindsey et al., 2023), indicating that the crustal anisotropy in this area is primarily controlled by geological structures (e.g., Boness & Zoback, 2006; T. Y. Huang et al., 2015; Johnson et al., 2011). Conversely, at stations C11 and SIM in the southern IBR, the crustal fast orientations are perpendicular to the structural trend of the mountain range (Figure 5) but align with the direction of compressive strain (Lindsey et al., 2023), indicating that the crustal anisotropy at these stations is dominated by stress rather than geological structures. Under stress-dominated conditions, microcracks in the crust that are perpendicular to the direction of maximum horizontal stress tend to close, causing the crustal fast orientations to align with the direction of maximum horizontal stress, which corresponds to the direction of compressive strain (e.g., Crampin & Peacock, 2008; Leary et al., 1990). Notably, Station C11 exhibits a large delay time of 0.68 s, which is significantly higher than the average crustal delay time of approximately 0.2 s reported in previous studies (e.g., Savage, 1999; Silver, 1996). Crampin (1994) noted that heavily fractured rocks can produce shear-wave anisotropy exceeding 10%. The proximity of Station C11 to the plate convergence boundary suggests that the region is subjected to strong compressional stress, which may enhance crustal fracturing and explain the observed large delay time. For a 10% crustal anisotropy, a 0.68 s delay time requires an ∼20 km thick layer, which is less than the previously reported crustal thickness of ∼30 km in this area (Nwe et al., 2022), suggesting that the large delay time can be attributed to stress-induced micro-fractures in the upper and mid crust.

The transition in crustal fast orientations from parallel to the structural trend of the IBR in the north to perpendicular in the south, accompanied by a southward decrease in XKS splitting times (Figure 5), reflects the coexistence of structure-induced and stress-induced crustal anisotropy in the IBR. In the northern IBR, where larger XKS splitting times are observed, the region is farther from the plate convergent boundary and features higher and wider mountain ranges (Morley et al., 2020) compared to the southern IBR (Figure 5). These observations suggest that the northern IBR is influenced by relatively weaker compressive stress caused by plate convergence but stronger geological structural factors, leading to structure-induced crustal anisotropy. Conversely, at stations C11 and SIM in the southern IBR, which are closer to the plate convergent boundary and characterized by lower and narrower mountain ranges (Figure 5), stress-induced crustal anisotropy dominates due to stronger compressive stress and weaker structural influences.

Despite these findings, our interpretation has some limitations, primarily due to the sparse spatial distribution of seismic stations with reliable crustal anisotropy measurements. In areas lacking such measurements, it remains premature to conclude that N-S oriented, structure-induced crustal anisotropy is uniformly present throughout the northern IBR. Local SWS measurements from direct S-waves, with focal depths of 20–40 km in the northern IBR, where large XKS splitting times have been observed, yielded average crustal splitting times of only 0.05 ± 0.02 s (Mohanty et al., 2024). These much smaller splitting times, compared to the average XKS splitting time of 2.09 ± 0.55 s reported by Fan et al. (2021), suggest that crustal anisotropy accounts for only a small portion of the observed XKS splitting. This indicates weak crustal anisotropy in parts of the northern IBR. Similarly, nearly isotropic crustal properties were observed at Station E01 in the southern IBR (Figure 5).

4.3. Combined Effects of Absolute Plate Motion, Indian Plate Subduction, and Remnant Neo-Tethyan Slab on Mantle Flow

The estimated depths of anisotropy indicate that beneath the IBR and the WBT, anisotropy originates mainly from the sub-slab mantle. In these areas, the observed XKS fast orientations predominantly align with the strike of the slab, reflecting trench-parallel mantle flow beneath the slab (Fan et al., 2021; Islam et al., 2024). However, east of the WBT, as the subduction depth of the Indian plate increases, the contribution of trench-parallel flow beneath the slab to anisotropy gradually diminishes (Figure 6). The estimated depth of anisotropy indicates that in the combined region of the Mogok Metamorphic Belt and ST, the anisotropy mainly originates from the mantle wedge above the subducting slab, suggesting a transition in the dominant source of anisotropy from the sub-slab mantle in the WBT to the mantle wedge above the slab in the Mogok Metamorphic Belt and ST (Figure 6). This

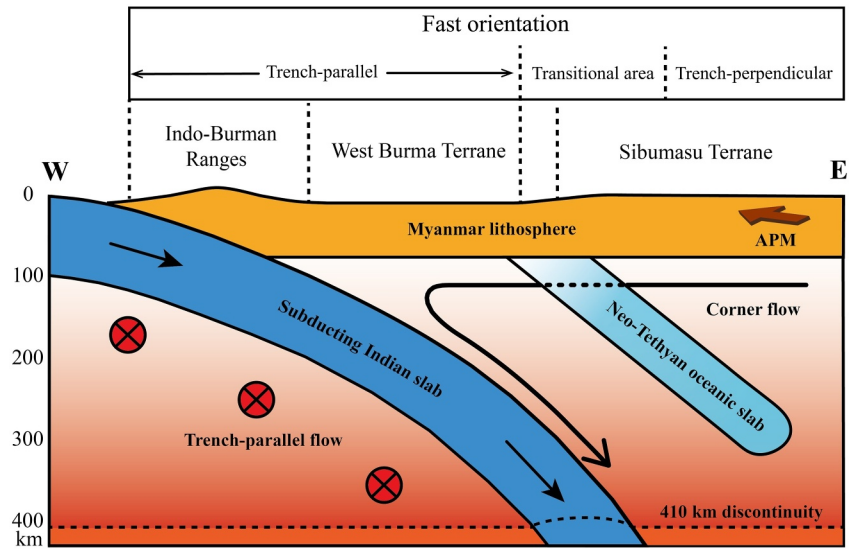

Figure 6. Schematic W-E cross-sectional diagram showing the tectonic framework and mantle flow patterns beneath Myanmar. The upper panel displays the spatial distribution of the Indo-Burman Ranges, West Burma Terrane, and Sibumasu Terrane with their associated fast orientation characteristics. The brown arrow indicates the absolute plate motion direction of the Eurasian plate at approximately −78° relative to geographic north. The double subduction system (Yang et al., 2022) comprises the subducting Indian slab (dark blue) and the remnant Neo-Tethyan oceanic slab (light blue). The black arrow above the subducting Indian slab indicates trench-perpendicular corner flow in the mantle wedge. The dashed segment of the black arrow, passing through the remnant Neo-Tethyan oceanic slab, indicates that the slab is permeable to mantle flow. Red crosses denote trench-parallel flow beneath the subducting Indian slab.

transition is further supported by the observed changes in XKS fast orientations within the ST. In the western ST, the fast orientations remain trench-parallel, but further east, north of 19.5°N, the fast orientations progressively rotate counterclockwise, approaching a near trench-perpendicular orientation. South of 19.5°N, an abrupt 90° rotation occurs (Figure 5a).

Although B-type olivine fabric has been suggested to occur in the forearc mantle wedge in Myanmar (Fan et al., 2024), its presence beneath the ST, where transitional XKS fast orientations are observed (Figure 5), is unlikely. B-type olivine fabric typically forms under relatively low-temperature, high-stress, and water-rich conditions (e.g., Karato et al., 2008). In contrast, the ST is located in the back-arc region, where temperatures are relatively higher and stresses are lower than in the forearc. These conditions are unfavorable for the development of B-type fabric. Therefore, the observed transitional fast orientations are more likely attributed to other types of olivine fabrics.

Previous studies have attributed the fast orientations in the northwestern ST to the corner flow induced by the Indian slab subduction and rollback (Fan et al., 2021), while the trench-perpendicular E-W fast orientations south of 19.5°N in the ST have been interpreted as resulting from trench-perpendicular flow driven by slab rollback (Yu et al., 2018). It is worth noting that the slab rollback model proposed by Yu et al. (2018) was based on the limited GPS data available at the time. Due to the lack of geodetic constraints south of 19.5°N, the presence of active subduction in this region remained uncertain, and slab rollback was considered a more plausible explanation for the observed anisotropy. Updated geodetic studies confirm that the subduction of the Indian Plate is active (Lindsey et al., 2023; Mallick et al., 2019; Steckler et al., 2016). Although the maximum convergence rate of approximately 24 mm/yr between the Indian and Eurasian plates (Mallick et al., 2019) is relatively low compared to other subduction zones (Long & Wirth, 2013) and may not readily generate extensive corner flow, slab rollback can facilitate trench-perpendicular mantle flow under such conditions. Therefore, the nearly E-W fast orientations south of 19.5°N in the ST (Figure 5a) can be attributed to trench-perpendicular corner flow induced by active subduction, potentially enhanced by slab rollback, though its occurrence in this region is not yet fully resolved.

Islam et al. (2024) proposed that one possible explanation for the XKS fast orientations in the Indochina Peninsula is shear of the lithosphere on the asthenosphere driven by APM, producing fast orientations parallel to the APM

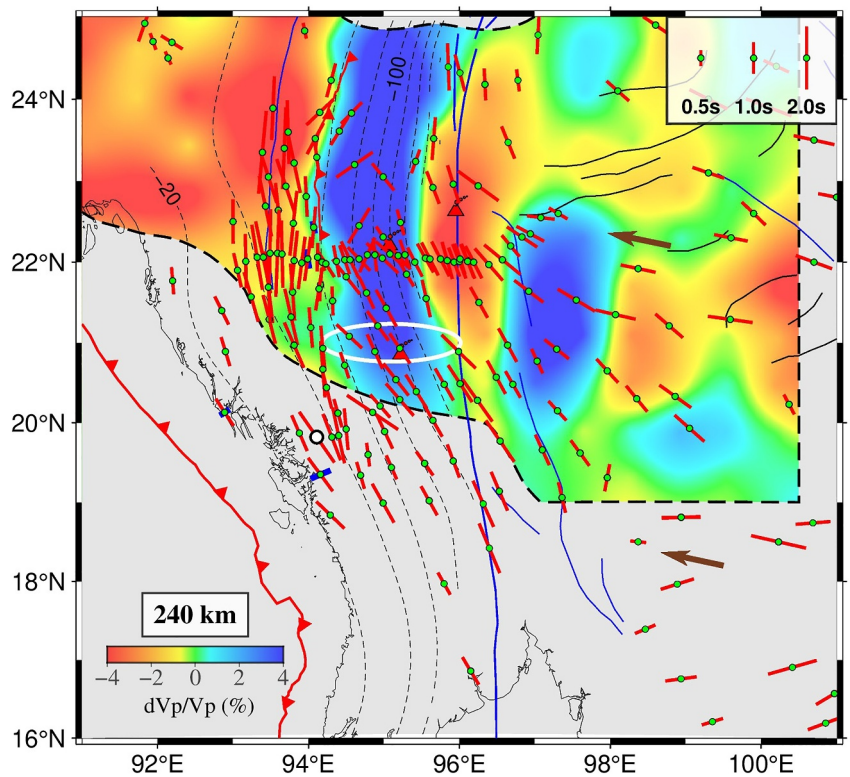

Figure 7. Comparison between station-averaged XKS splitting measurements and P-wave velocity anomalies at a depth of 240 km (Yang et al., 2022). The splitting measurements are from this study and previous studies (Fan et al., 2021; Islam et al., 2024; Liu et al., 2019; Shi et al., 2012; Yu et al., 2018). The high P-wave velocity anomaly in the east represents the remnant of the subducted Neo-Tethyan oceanic slab, while the western anomaly corresponds to the subducting Indian slab. The area marked by the white ellipse indicates the location of a potential slab tear (Bai et al., 2020). For additional information and labels, please refer to Figures 1 and 5.

direction. However, the nearly E-W fast orientations in the southern ST do not align with the APM direction, whereas in the northern ST, the fast orientations align with the APM direction (Figure 5a). This suggests that APM-driven flow predominantly governs anisotropy in the northern ST.

Interestingly, the transitional XKS fast orientations between the APM-parallel fast orientations in the northern ST and the nearly E-W fast orientations in the southern ST align with neither the APM direction nor the trench-perpendicular direction (Figure 5a). This transitional pattern, marked by a progressively counterclockwise rotation in fast orientations from trench-parallel in the west to nearly trench-perpendicular in the east within the ST, cannot be explained solely by either APM-driven flow or trench-perpendicular corner flow. Additionally, teleseismic tomography by Yang et al. (2022) has identified a remnant subducted Neo-Tethyan oceanic slab beneath the fast orientation transitional zone in the ST (Figure 7). We propose that the region with transitional fast orientations is influenced by a combination of three factors: corner flow induced by active subduction, APM-driven mantle flow, and the remnant Neo-Tethyan slab (Figure 6).

4.4. The Nature of the Neo-Tethyan Oceanic Slab and Constraints on the Slab Tear

Teleseismic tomography reveals that the remnant Neo-Tethyan oceanic slab beneath the ST extends to a depth of approximately 300 km, dipping eastward (Yang et al., 2022). The collision between the WBT and the ST around 40 Ma (Westerweel et al., 2019) marked a transition from active to stagnant subduction of the Neo-Tethyan oceanic lithosphere. The remnant slab may now act as a barrier, impeding mantle flow across it and potentially driving slab-parallel mantle flow. However, fast orientations parallel to the slab strike are not observed near the remnant slab. Instead, the fast orientations are oblique to the slab strike (Figure 7). Similar patterns of fast orientations oblique to the strike of the subducting slab have been reported in the Cocos slab beneath Central America, where the obliquity has been attributed to slab fragmentation, allowing mantle material to flow across

the slab (Xue et al., 2023). In the case of the Neo-Tethyan remnant slab, the high P-wave velocity anomaly associated with the remnant slab appears to diminish within the depth range of 50–125 km (Yang et al., 2022). This reduction in velocity suggests that the remnant slab may have weakened at these depths, becoming permeable to mantle flow rather than acting as a rigid barrier (Figure 6). The estimated depth of anisotropy in the ST (125 km) aligns with the depth range of the reduced P-wave velocity anomaly, supporting the interpretation that the remnant slab is permeable. Additionally, slight variations in splitting times observed along different parts of the remnant slab suggest that its permeability to mantle flow may vary spatially (Figure 7).

Previous receiver function images at ∼21°N reveal distinct variations in mantle transition zone discontinuities (Bai et al., 2020), attributed to a tear in the subducting Indian slab (Figure 7). This slab tear may enable the upwelling of hot asthenospheric material, possibly leading to Quaternary volcanism in the WBT (Sano et al., 2022). Typically, slab windows can allow material beneath the subducting slab to flow into the mantle wedge, leading to trench-perpendicular flow and upwelling, which can result in trench-perpendicular fast orientations (e.g., Kong et al., 2022; Lynner et al., 2017) or null measurements indicative of isotropy (e.g., Wu et al., 2019). However, in the IBR and the WBT near 21°N, the observed XKS fast orientations are parallel to the slab strike rather than trench-perpendicular (Figure 7). This challenges the presence of significant trench-perpendicular mantle flow and upwelling through the slab window, implying that the slab tear may be narrow and insufficient to disrupt the prevailing trench-parallel sub-slab mantle flow in this region.

5. Conclusions

Taking advantage of the new seismic data from the second phase of the CMGSMO array, we conducted SWS analysis of XKS phases in central Myanmar, estimated the depth of anisotropy, and investigated the crustal anisotropy in the IBR. Our findings provide new insights into the crustal deformation mechanisms and mantle flow patterns in this tectonically complex subduction zone:

1. Variations in XKS splitting times across the IBR are primarily due to differences in crustal anisotropy. In the northern part of the IBR, the N-S oriented crustal anisotropy is primarily induced by the N-S trending geological structures. In contrast, the trench-perpendicular crustal anisotropy in the southern part of the IBR is stress-induced, aligning with the direction of compression caused by plate convergence.
2. There is a transition in the primary source of anisotropy, from beneath the subducting slab in the WBT to the mantle wedge above the slab in the ST.
3. In the ST, the transitional XKS fast orientations are shaped by a combination of factors, including corner flow induced by active subduction, APM-driven flow, and the influence of the remnant Neo-Tethyan slab, which is permeable to mantle flow at depths of 50–125 km.
4. Near 21°N, the XKS fast orientations remain consistently trench-parallel, indicating that the width of the slab tear is limited and has minimal impact on mantle flow patterns.

Conflict of Interest

The authors declare no conflicts of interest relevant to this study.

Data Availability Statement

The waveform data used for shear wave splitting analysis in this study, collected from the recently deployed second phase of the CMGSMO seismic array, along with the acquired radial P-wave receiver functions and splitting measurements, are available at Fan et al. (2025). Other data are publicly available from the Seismological Facility for the Advancement of Geoscience (SAGE). Station-averaged splitting parameters are provided in Table S1.

Acknowledgments
We thank all participants in the second phase of the CMGSMO project for their efforts in installing and maintaining the seismic network. Our gratitude also goes to Editor Fenglin Niu, the Associate Editor, Reviewer Zhouchuan Huang, and an anonymous reviewer for their constructive comments. Most figures were generated using the Generic Mapping Tools (Wessel et al., 2019). This study was supported by the National Natural Science Foundation of China (Grants 42304107, 42030309, and 42130308). Data analysis was partially supported by the United States National Science Foundation (awards 1919789 and 2149587).

References

Almqvist, B. S. G., & Mainprice, D. (2017). Seismic properties and anisotropy of the continental crust: Predictions based on mineral texture and rock microstructure. *Reviews of Geophysics*, *55*(2), 367–433. https://doi.org/10.1002/2016rg000552

Appini, S., Li, J., Hu, H., Creasy, N., Thomsen, L., McNease, J., & Zheng, Y. (2025). Prediction of complex observed shear wave splitting patterns at Ryukyu subduction zone using a strong intra-slab anisotropy model. *Geophysical Research Letters*, *52*(3), e2024GL111131. https://doi.org/10.1029/2024gl111131

Bai, Y., He, Y., Yuan, X., Tilmann, F., Ai, Y., Jiang, M., et al. (2021). Seismic structure across central Myanmar from joint inversion of receiver functions and Rayleigh wave dispersion. *Tectonophysics*, *818*, 229068. https://doi.org/10.1016/j.tecto.2021.229068

Bai, Y., Yuan, X., He, Y., Hou, G., Thant, M., Sein, K., & Ai, Y. (2020). Mantle transition zone structure beneath Myanmar and its geodynamic implications. *Geochemistry, Geophysics, Geosystems*, *21*(12), e2020GC009262. https://doi.org/10.1029/2020gc009262

Boness, N. L., & Zoback, M. D. (2006). Mapping stress and structurally controlled crustal shear velocity anisotropy in California. *Geology*, *34*(10), 825–828. https://doi.org/10.1130/G22309.1

Cai, F., Ding, L., Yao, W., Laskowski, A. K., Xu, Q., Zhang, J. E., & Sein, K. (2017). Provenance and tectonic evolution of lower paleozoic-upper Mesozoic strata from Sibumasu terrane, Myanmar. *Gondwana Research*, *41*, 325–336. https://doi.org/10.1016/j.gr.2015.03.005

Crampin, S. (1994). The fracture criticality of crustal rocks. *Geophysical Journal International*, *118*(2), 428–438. https://doi.org/10.1111/j.1365-246X.1994.tb03974.x

Crampin, S., & Peacock, S. (2008). A review of the current understanding of seismic shear-wave splitting in the Earth's crust and common fallacies in interpretation. *Wave Motion*, *45*(6), 675–722. https://doi.org/10.1016/j.wavemoti.2008.01.003

Fan, E., Ai, Y., Gao, S. S., He, Y., Liu, K. H., Jiang, M., et al. (2024). Mantle flow and olivine fabric transition in the Myanmar continental subduction zone. *Geology*, *52*(4), 225–229. https://doi.org/10.1130/G51698.1

Fan, E., He, Y., Ai, Y., Gao, S. S., Liu, K. H., Jiang, M., et al. (2021). Seismic anisotropy and mantle flow constrained by shear wave splitting in central Myanmar. *Journal of Geophysical Research: Solid Earth*, *126*(10), e2021JB022144. https://doi.org/10.1029/2021JB022144

Fan, E., Jiang, M., Ai, Y., Gao, S. S., Liu, K. H., He, Y., et al. (2025). Mantle flow and crustal deformation revealed by seismic anisotropy in the subduction zone beneath Myanmar [Dataset]. *WDC for Geophysics, Beijing*. https://doi.org/10.12197/2025GA001

Gahalaut, V. K., Kundu, B., Laishram, S. S., Catherine, J., Kumar, A., Singh, M. D., et al. (2013). Aseismic plate boundary in the Indo-Burmese wedge, northwest Sunda Arc. *Geology*, *41*(2), 235–238. https://doi.org/10.1130/G33771.1

Gao, S. S., Liu, K. H., & Abdelsalam, M. G. (2010). Seismic anisotropy beneath the Afar depression and adjacent areas: Implications for mantle flow. *Journal of Geophysical Research*, *115*(B12), B12330. https://doi.org/10.1029/2009jb007141

Garzanti, E., Limonta, M., Resentini, A., Bandopadhyay, P. C., Najman, Y., Andò, S., & Vezzoli, G. (2013). Sediment recycling at convergent plate margins (Indo-Burman ranges and Andaman-Nicobar ridge). *Earth-Science Reviews*, *123*, 113–132. https://doi.org/10.1016/j.earscirev.2013.04.008

Gerst, A. (2003). *Temporal changes in seismic anisotropy as a new eruption forecasting tool*. (Master's thesis). Retrieved from Open Access Te Herenga Waka-Victoria University of Wellington. https://doi.org/10.26686/wgtn.16910776.v1

Gripp, A. E., & Gordon, R. G. (2002). Young tracks of hotspots and current plate velocities. *Geophysical Journal International*, *150*(2), 321–361. https://doi.org/10.1046/j.1365-246X.2002.01627.x

Guillaume, B., Moroni, M., Funiciello, F., Martinod, J., & Faccenna, C. (2010). Mantle flow and dynamic topography associated with slab window opening: Insights from laboratory models. *Tectonophysics*, *496*(1), 83–98. https://doi.org/10.1016/j.tecto.2010.10.014

Hayes, G. P., Moore, G. L., Portner, D. E., Hearne, M., Flamme, H., Furtney, M., & Smoczyk, G. M. (2018). Slab2, a comprehensive subduction zone geometry model. *Science*, *362*(6410), 58–61. https://doi.org/10.1126/science.aat4723

Huang, T. Y., Gung, Y., Kuo, B. Y., Chiao, L. Y., & Chen, Y. N. (2015). Layered deformation in the Taiwan orogen. *Science*, *349*(6249), 720–723. https://doi.org/10.1126/science.aab1879

Huang, Z., Tilmann, F., Xu, M., Wang, L., Ding, Z., Mi, N., et al. (2017). Insight into NE Tibetan Plateau expansion from crustal and upper mantle anisotropy revealed by shear-wave splitting. *Earth and Planetary Science Letters*, *478*, 66–75. https://doi.org/10.1016/j.epsl.2017.08.030

Huang, Z., Wang, L., Xu, M., Ding, Z., Wu, Y., Wang, P., et al. (2015). Teleseismic shear-wave splitting in SE Tibet: Insight into complex crust and upper-mantle deformation. *Earth and Planetary Science Letters*, *432*, 354–362. https://doi.org/10.1016/j.epsl.2015.10.027

Huang, Z., Zhao, D., & Wang, L. (2011). Shear wave anisotropy in the crust, mantle wedge, and subducting Pacific slab under northeast Japan. *Geochemistry, Geophysics, Geosystems*, *12*(1), Q01002. https://doi.org/10.1029/2010gc003343

Hurukawa, N., Tun, P. P., & Shibazaki, B. (2012). Detailed geometry of the subducting Indian plate beneath the Burma plate and subcrustal seismicity in the Burma plate derived from joint hypocenter relocation. *Earth Planets and Space*, *64*(4), 333–343. https://doi.org/10.5047/eps.2011.10.011

Islam, M. M., Wei, S., Persaud, P., Steckler, M. S., Tilmann, F., Ni, J., et al. (2024). Mantle deformation in the highly oblique Indo-Burma subduction system inferred from shear wave splitting measurements. *Earth and Planetary Science Letters*, *643*, 118895. https://doi.org/10.1016/j.epsl.2024.118895

Johnson, J. H., Savage, M. K., & Townend, J. (2011). Distinguishing between stress-induced and structural anisotropy at Mount Ruapehu volcano, New Zealand. *Journal of Geophysical Research*, *116*(B12), B12303. https://doi.org/10.1029/2011jb008308

Karato, S.-I., Jung, H., Katayama, I., & Skemer, P. (2008). Geodynamic significance of seismic anisotropy of the upper mantle: New insights from laboratory studies. *Annual Review of Earth and Planetary Sciences*, *36*(1), 59–95. https://doi.org/10.1146/annurev.earth.36.031207.124120

Kong, F., Gao, S. S., Liu, K. H., & Li, J. (2022). Potassic volcanism induced by mantle upwelling through a slab window: Evidence from shear wave splitting analyses in central java. *Journal of Geophysical Research: Solid Earth*, *127*(3), e2021JB023719. https://doi.org/10.1029/2021jb023719

Kong, F., Wu, J., Liu, L., Liu, K. H., Song, J., Li, J., & Gao, S. S. (2018). Azimuthal anisotropy and mantle flow underneath the southeastern Tibetan Plateau and northern Indochina Peninsula revealed by shear wave splitting analyses. *Tectonophysics*, *747–748*, 68–78. https://doi.org/10.1016/j.tecto.2018.09.013

Leary, P. C., Crampin, S., & McEvilly, T. V. (1990). Seismic fracture anisotropy in the Earth's crust: An overview. *Journal of Geophysical Research*, *95*(B7), 11105–11114. https://doi.org/10.1029/JB095iB07p11105

Lee, H.-Y., Chung, S.-L., & Yang, H.-M. (2016). Late Cenozoic volcanism in central Myanmar: Geochemical characteristics and geodynamic significance. *Lithos*, *245*, 174–190. https://doi.org/10.1016/j.lithos.2015.09.018

Li, C., van der Hilst, R. D., Meltzer, A. S., & Engdahl, E. R. (2008). Subduction of the Indian lithosphere beneath the Tibetan Plateau and Burma. *Earth and Planetary Science Letters*, *274*(1–2), 157–168. https://doi.org/10.1016/j.epsl.2008.07.016

Lindsey, E. O., Wang, Y., Aung, L. T., Chong, J.-H., Qiu, Q., Mallick, R., et al. (2023). Active subduction and strain partitioning in western Myanmar revealed by a dense survey GNSS network. *Earth and Planetary Science Letters*, *622*, 118384. https://doi.org/10.1016/j.epsl.2023.118384

Liu, K. H., & Gao, S. S. (2013). Making reliable shear-wave splitting measurements. *Bulletin of the Seismological Society of America*, *103*(5), 2680–2693. https://doi.org/10.1785/0120120355

Liu, K. H., Gao, S. S., Gao, Y., & Wu, J. (2008). Shear wave splitting and mantle flow associated with the deflected Pacific slab beneath northeast Asia. *Journal of Geophysical Research*, *113*(B1), B01305. https://doi.org/10.1029/2007jb005178

Liu, L., Gao, S. S., Liu, K. H., Li, S., Tong, S., & Kong, F. (2019). Toroidal mantle flow induced by slab subduction and rollback beneath the eastern Himalayan syntaxis and adjacent areas. *Geophysical Research Letters*, *46*(20), 11080–11090. https://doi.org/10.1029/2019gl084961

Liu, X., & Pysklywec, R. (2023). Transient injection of flow: How torn and bent slabs induce unusual mantle circulation patterns near a flat slab. *Geochemistry, Geophysics, Geosystems*, *24*(10), e2023GC011056. https://doi.org/10.1029/2023GC011056

Long, M. D., & Wirth, E. A. (2013). Mantle flow in subduction systems: The mantle wedge flow field and implications for wedge processes. *Journal of Geophysical Research: Solid Earth*, *118*(2), 583–606. https://doi.org/10.1002/jgrb.50063

Lynner, C., Anderson, M. L., Portner, D. E., Beck, S. L., & Gilbert, H. (2017). Mantle flow through a tear in the Nazca slab inferred from shear wave splitting. *Geophysical Research Letters*, *44*(13), 6735–6742. https://doi.org/10.1002/2017GL074312

Mallick, R., Lindsey, E. O., Feng, L., Hubbard, J., Banerjee, P., & Hill, E. M. (2019). Active convergence of the India-Burma-Sunda plates revealed by a new continuous GPS network. *Journal of Geophysical Research: Solid Earth*, *124*(3), 3155–3171. https://doi.org/10.1029/2018jb016480

Mohanty, D. D., Biswal, S., & Yoshizawa, K. (2024). Decoupled deformation between crust and mantle beneath Indo-Burmese wedge: A new seismotectonic model. *Earth and Planetary Science Letters*, *648*, 119089. https://doi.org/10.1016/j.epsl.2024

Mon, C. T., Gong, X., Wen, Y., Jiang, M., Chen, Q. F., Zhang, M., et al. (2020). Insight into major active faults in central Myanmar and the related geodynamic sources. *Geophysical Research Letters*, *47*(8), e2019GL086236. https://doi.org/10.1029/2019gl086236

Mon, C. T., Yang, S., Ren, C., He, Y., Thant, M., & Sein, K. (2023). New insight into the subducted Indian Plate beneath central Myanmar based on seismic activity and focal mechanisms analysis. *Seismological Research Letters*, *94*(5), 2337–2347. https://doi.org/10.1785/0220220381

Morley, C. K. (2018). Understanding Sibumasu in the context of ribbon continents. *Gondwana Research*, *64*, 184–215. https://doi.org/10.1016/j.gr.2018.07.006

Morley, C. K., Chantraprasert, S., Kongchum, J., & Chenoll, K. (2021). The West Burma Terrane, a review of recent paleo-latitude data, its geological implications and constraints. *Earth-Science Reviews*, *220*, 103722. https://doi.org/10.1016/j.earscirev.2021.103722

Morley, C. K., Tin Tin, N., Searle, M., & Robinson, S. A. (2020). Structural and tectonic development of the Indo-Burma ranges. *Earth-Science Reviews*, *200*, 102992. https://doi.org/10.1016/j.earscirev.2019.102992

Nwe, L., Wei, Z., Li, Z., Bao, F., Li, X., & Hu, J. (2022). Crustal thickness, Vp/Vs ratio, and shear wave velocity structures beneath Myanmar and their tectonic implications. *Earthquake Research Advances*, *2*(1), 100060. https://doi.org/10.1016/j.eqrea.2021.100060

Pasyanos, M. E., Masters, T. G., Laske, G., & Ma, Z. (2014). LITHO1.0: An updated crust and lithospheric model of the Earth. *Journal of Geophysical Research: Solid Earth*, *119*(3), 2153–2173. https://doi.org/10.1002/2013jb010626

Paul, A., Karabulut, H., Mutlu, A. K., & Salaün, G. (2014). A comprehensive and densely sampled map of shear-wave azimuthal anisotropy in the Aegean-Anatolia region. *Earth and Planetary Science Letters*, *389*, 14–22. https://doi.org/10.1016/j.epsl.2013.12.019

Sano, T., Tani, K., Yoneda, S., Min, H., Htike, T., Maung Thein, Z. M., et al. (2022). Petrogenesis of isotopically enriched Quaternary magma with adakitic affinity associated with subduction of old lithosphere beneath central Myanmar. *Scientific Reports*, *12*(1), 3137. https://doi.org/10.1038/s41598-022-07097-4

Savage, M. K. (1999). Seismic anisotropy and mantle deformation: What have we learned from shear wave splitting? *Reviews of Geophysics*, *37*(1), 65–106. https://doi.org/10.1029/98RG02075

Searle, M. P., Morley, C. K., Waters, D. J., Gardiner, N. J., Kyi Htun, U., Nu, T. T., & Robb, L. J. (2017). Tectonic and metamorphic evolution of the Mogok Metamorphic and Jade Mines belts and ophiolitic terranes of Burma (Myanmar). In A. J. Barber, K. Zaw, & M. J. Crow (Eds.), *Myanmar: Geology, resources and tectonics* (pp. 261–293). Geological Society of London.

Shi, Y., Gao, Y., Su, Y., & Wang, Q. (2012). Shear-wave splitting beneath Yunnan area of Southwest China. *Earthquake Science*, *25*(1), 25–34. https://doi.org/10.1007/s11589-012-0828-4

Silver, P. G. (1996). Seismic anisotropy beneath the continents: Probing the depths of geology. *Annual Review of Earth and Planetary Sciences*, *24*(1), 385–432. https://doi.org/10.1146/annurev.earth.24.1.385

Silver, P. G., & Chan, W. W. (1991). Shear wave splitting and subcontinental mantle deformation. *Journal of Geophysical Research*, *96*(B10), 16429–16454. https://doi.org/10.1029/91jb00899

Silver, P. G., & Savage, M. K. (1994). The interpretation of shear-wave splitting parameters in the presence of two anisotropic layers. *Geophysical Journal International*, *119*(3), 949–963. https://doi.org/10.1111/j.1365-246X.1994.tb04027.x

Steckler, M. S., Mondal, D. R., Akhter, S. H., Seeber, L., Feng, L., Gale, J., et al. (2016). Locked and loading megathrust linked to active subduction beneath the Indo-Burman ranges. *Nature Geoscience*, *9*(8), 615–618. https://doi.org/10.1038/ngeo2760

Walsh, E., Arnold, R., & Savage, M. K. (2013). Silver and Chan revisited. *Journal of Geophysical Research: Solid Earth*, *118*(10), 5500–5515. https://doi.org/10.1002/jgrb.50386

Wang, Y., Sieh, K., Tun, S. T., Lai, K.-Y., & Myint, T. (2014). Active tectonics and earthquake potential of the Myanmar region. *Journal of Geophysical Research: Solid Earth*, *119*(4), 3767–3822. https://doi.org/10.1002/2013jb010762

Wessel, P., Luis, J. F., Uieda, L., Scharroo, R., Wobbe, F., Smith, W. H. F., & Tian, D. (2019). The generic mapping tools version 6. *Geochemistry, Geophysics, Geosystems*, *20*(11), 5556–5564. https://doi.org/10.1029/2019GC008515

Westerweel, J., Roperch, P., Licht, A., Dupont-Nivet, G., Win, Z., Poblete, F., et al. (2019). Burma Terrane part of the Trans-Tethyan arc during collision with India according to palaeomagnetic data. *Nature Geoscience*, *12*(10), 863–868. https://doi.org/10.1038/s41561-019-0443-2

Wu, C., Tian, X., Xu, T., Liang, X., Chen, Y., Taylor, M., et al. (2019). Deformation of crust and upper mantle in central Tibet caused by the northward subduction and slab tearing of the Indian lithosphere: New evidence based on shear wave splitting measurements. *Earth and Planetary Science Letters*, *514*, 75–83. https://doi.org/10.1016/j.epsl.2019.02.037

Xue, T., Peng, D., Liu, K. H., Obrist-Farner, J., Locmelis, M., Gao, S. S., & Liu, L. (2023). Ongoing fragmentation of the subducting cocos slab, Central America. *Geology*, *51*(12), 1106–1110. https://doi.org/10.1130/G51403.1

Yang, S., Liang, X., Jiang, M., Chen, L., He, Y., Thet Mon, C., et al. (2022). Slab remnants beneath the Myanmar terrane evidencing double subduction of the Neo-Tethyan Ocean. *Science Advances*, *8*(34), eabo1027. https://doi.org/10.1126/sciadv.abo1027

Yao, J., Liu, S., Wei, S., Hubbard, J., Huang, B. S., Chen, M., & Tong, P. (2021). Slab models beneath central Myanmar revealed by a joint inversion of regional and teleseismic traveltime data. *Journal of Geophysical Research: Solid Earth*, *126*(2), e2020JB020164. https://doi.org/10.1029/2020jb020164

Yu, Y., Gao, S. S., Liu, K. H., Yang, T., Xue, M., Le, K. P., & Gao, J. (2018). Characteristics of the mantle flow system beneath the Indochina Peninsula revealed by teleseismic shear wave splitting analysis. *Geochemistry, Geophysics, Geosystems*, *19*(5), 1519–1532. https://doi.org/10.1029/2018GC007474

Zhang, G., He, Y., Ai, Y., Jiang, M., Mon, C. T., Hou, G., et al. (2021). Indian continental lithosphere and related volcanism beneath Myanmar: Constraints from local earthquake tomography. *Earth and Planetary Science Letters*, *567*, 116987. https://doi.org/10.1016/j.epsl.2021.116987

Zheng, T., He, Y., Ding, L., Jiang, M., Ai, Y., Mon, C. T., et al. (2020). Direct structural evidence of Indian continental subduction beneath Myanmar. *Nature Communications*, *11*(1), 1944. https://doi.org/10.1038/s41467-020-15746-3

References From the Supporting Information

Ammon, C. J. (1991). The isolation of receiver effects from teleseismic P waveforms. *Bulletin of the Seismological Society of America*, *81*(6), 2504–2510. https://doi.org/10.1785/BSSA0810062504

Gao, S. S., & Liu, K. H. (2012). AnisDep: A FORTRAN program for the estimation of the depth of anisotropy using spatial coherency of shear-wave splitting parameters. *Computers and Geosciences*, *49*, 330–333. https://doi.org/10.1016/j.cageo.2012.01.020

Gao, S. S., & Liu, K. H. (2014). Mantle transition zone discontinuities beneath the contiguous United States. *Journal of Geophysical Research: Solid Earth*, *119*(8), 6452–6468. https://doi.org/10.1002/2014jb011253

Kong, F., Wu, J., Liu, K. H., & Gao, S. S. (2016). Crustal anisotropy and ductile flow beneath the eastern Tibetan Plateau and adjacent areas. *Earth and Planetary Science Letters*, *442*, 72–79. https://doi.org/10.1016/j.epsl.2016.03.003

Liu, K. H., & Gao, S. S. (2010). Spatial variations of crustal characteristics beneath the Hoggar swell, Algeria, revealed by systematic analyses of receiver functions from a single seismic station. *Geochemistry, Geophysics, Geosystems*, *11*(8), Q08011. https://doi.org/10.1029/2010gc003091

Liu, K. H., & Gao, S. S. (2011). Estimation of the depth of anisotropy using spatial coherency of shear-wave splitting parameters. *Bulletin of the Seismological Society of America*, *101*(5), 2153–2161. https://doi.org/10.1785/0120100258

Refayee, H. A., Yang, B. B., Liu, K. H., & Gao, S. S. (2014). Mantle flow and lithosphere-asthenosphere coupling beneath the southwestern edge of the North American craton: Constraints from shear-wave splitting measurements. *Earth and Planetary Science Letters*, *402*, 209–220. https://doi.org/10.1016/j.epsl.2013.01.031

Rumpker, G., Kaviani, A., & Latifi, K. (2014). Ps-splitting analysis for multilayered anisotropic media by azimuthal stacking and layer stripping. *Geophysical Journal International*, *199*(1), 146–163. https://doi.org/10.1093/gji/ggu154

Zheng, T., Ding, Z., Ning, J., Chang, L., Wang, X., Kong, F., et al. (2018). Crustal azimuthal anisotropy beneath the southeastern Tibetan Plateau and its geodynamic implications. *Journal of Geophysical Research: Solid Earth*, *123*(11), 9733–9749. https://doi.org/10.1029/2018jb015995